Spatial separation of FtsZ and FtsN during cell division

Author	Bill Soderstrom, Helena Chan, Patrick J. Shilling, Ulf Skoglund, Daniel O. Daley
journal or publication title	Molecular Microbiology
volume	107
number	3
page range	387-401
year	2017-12-19
Publisher	John Wiley & Sons Ltd
Rights	(C) 2017 John Wiley & Sons Ltd This is the peer reviewed version of the following article: Soderstrom, B., Chan, H., Shilling, P. J., Skoglund, U and Daley, D. O (2018), Spatial separation of FtsZ and FtsN during cell division. Molecular Microbiology, 107: 387-401. doi:10.1111/mmi.13888, which has been published in final format https://doi.org/10.1111/mmi.13888. This article may be used for non-commercial purposes in accordance with Wiley Terms and Conditions for Use of Self-Archived Versions.
Author's flag	author
URL	http://id.nii.ac.jp/1394/00000366/

Spatial separation of FtsZ and FtsN during cell division

1

Spatial separation of FtsZ and FtsN

during cell division

4

Bill Söderström[1*], Helena Chan[1], Patrick J. Shilling[2],

Ulf Skoglund[1] and Daniel O. Daley[2*]

7

[1]Structural Cellular Biology Unit

Okinawa Institute of Science and Technology

Okinawa 904-0495

Japan

[2]Department of Biochemistry and Biophysics

Stockholm University,

Stockholm 106 91

Sweden

16

Address correspondence to:

Bill Söderström, bill.soederstroem@oist.jp; Tel +81 8064837515

Or

Daniel Daley, ddaley@dbb.su.se; Tel +46 8 162 910

21

22

Key words: *E. coli*, cell division, FtsZ, FtsN, super-resolution microscopy,

gSTED, SIM

25   **Summary**

26   The division of *Escherichia coli* is mediated by a collection of some 34

27   different proteins that are recruited to the division septum and are thought to

28   assemble into a macromolecular complex known as 'the divisome'. Herein we

29   have endeavored to better understand the structure of the divisome by

30   imaging two of its core components; FtsZ and FtsN. Super resolution

31   microscopy (SIM and gSTED) indicated that both proteins are localized in

32   large assemblies, which are distributed around the division septum (i.e.

33   forming a discontinuous ring). Although the rings had similar radii prior to

34   constriction, the individual densities were often spatially separated

35   circumferentially. As the cell envelope constricted, the discontinuous ring

36   formed by FtsZ moved inside the discontinuous ring formed by FtsN. The

37   radial and circumferential separation observed in our images indicates that

38   the majority of FtsZ and FtsN molecules are organized in different

39   macromolecular assemblies, rather than in large super-complex. This

40   conclusion was supported by Fluorescence Recovery After Photobleaching

41   (FRAP) measurements, which indicated that the dynamic behavior of the two

42   macromolecular assemblies was also fundamentally different. Taken together,

43   the data indicates that constriction of the cell envelope is brought about by (at

44   least) two spatially separated complexes.

Introduction

In *Escherichia coli*, at least thirty-four different proteins are recruited to the septum at the onset of division (de Boer, 2010). Ten of these proteins are thought to have major roles in constricting the mother cell and separating the daughter cells, as they are essential for cell viability (i.e. FtsZ, FtsA, ZipA, FtsK, FtsQ, FtsL, FtsB, FtsW, FtsI and FtsN) (Haeusser & Margolin, 2016, de Boer, 2010). Details of how the essential division proteins are recruited to the septum, a process often referred to as 'assembly', have been revealed through decades of research (den Blaauwen *et al.*, 2017). Thousands of molecules of FtsZ are corralled, then polymerized and bundled into filaments that are tethered to the inner membrane by FtsA and ZipA (Haeusser & Margolin, 2016, Erickson *et al.*, 2010). This intermediate structure is often referred to as the Z-ring (or proto-ring) on account of the fact that it resembles a ring when analyzed by fluorescence microscopy (Rowlett & Margolin, 2015). The Z-ring subsequently acts as an assembly platform for proteins involved in chromosome partitioning (e.g. FtsK) and peptidoglycan (PG) synthesis (e.g. FtsQ, FtsL, FtsW, FtsI, FtsN), which are recruited after a time delay (Aarsman *et al.*, 2005). Once all essential proteins have arrived at the septum, it is assumed that they assemble into a single macromolecular complex, which is referred to as the divisome (see (Trip & Scheffers, 2015) and references therein). Although the divisome has yet to be isolated, its existence is based on three main lines of evidence:

1. Experiments showing that the recruitment of proteins to the septum is often dependent on the existence of upstream proteins (Goehring & Beckwith, 2005).

70   2. Protein: protein interaction studies that indicate a high level of

71   connectivity between proteins (Alexeeva *et al.*, 2010, Egan &

72   Vollmer, 2013, Pazos *et al.*, 2013, Buddelmeijer & Beckwith, 2004,

73   Muller *et al.*, 2007, Fraipont *et al.*, 2011, Karimova *et al.*, 2005, Di

74   Lallo *et al.*, 2003).

75   3. The identification of a 1MDa complex containing some divisome

76   proteins (Trip & Scheffers, 2015).

77 Constriction of the cell envelope begins once FtsN has arrived at the division

78 septum (Weiss, 2015). It is powered by the constriction of FtsZ polymers in

79 the cytoplasm (Osawa *et al.*, 2008, Osawa *et al.*, 2009, Osawa & Erickson,

80 2013), and the inward growth of the PG layer in the periplasm (Meier & Goley,

81 2014, den Blaauwen *et al.*, 2017, Xiao & Goley, 2016, Coltharp & Xiao, 2017).

82 A compelling model for how the constriction of FtsZ polymers and PG

83 synthesis are coordinated has been recently proposed (Yang *et al.*, 2017).

84 This model postulates that FtsZ polymers swirl around the division site using a

85 treadmilling mechanism. The treadmilling of FtsZ modulates the

86 circumferential speed of proteins involved in PG synthesis, resulting in the in-

87 growth of PG at sites where FtsZ polymers are actively constricting. Currently

88 the molecular mechanism(s) by which the Z-ring modulates the PG

89 synthesizing machinery is not understood, but it is implied that they are

90 physically connected (Yang *et al.*, 2017, Schoenemann & Margolin, 2017).

91 High-resolution information on the structural architecture of the divisome

92 would help to determine if FtsZ is in fact physically coupled to the PG

93 synthesizing machinery. Our current view of the divisome structure is based

94 on super-resolution imaging of fluorescently labeled FtsZ, FtsA and ZipA,

95   which revealed that these three proteins form patchy ring structures, with

96   bead-like densities that often overlap (Strauss *et al.*, 2012, Rowlett &

97   Margolin, 2014). The bead-like densities represent filaments that are each ~

98   100 nm long and that together span the circumference of the septum

99   (Coltharp *et al.*, 2016). It has been largely assumed that other divisome

100   proteins are physically associated with these filaments throughout

101   constriction. However, recent studies have suggested that proteins in the Z-

102   ring are spatially separated from and proteins involved in PG synthesis

103   machinery (Söderström *et al.*, 2016, Buss *et al.*, 2015). Our goals in this study

104   were to confirm this separation, to determine when it happened, and better

105   understand how it affected the ability of the Z-ring to co-ordinate the

106   localization of the PG synthesizing machinery.

107

108   **Results**

109   *The Z-ring and the PG synthesizing machinery are visibly separated at the*

110   *septum*

111   To confirm that the Z-ring and the PG synthesizing machinery were separated

112   at the septum during constriction, we ectopically expressed FtsZ-GFP (a

113   marker for the Z-ring) and mCherry-FtsN (a marker for the PG synthesizing

114   machinery) in the *E. coli* strain MG1655. Live cells were then trapped in

115   microholes made in agarose beds as previously described (Bisson-Filho *et al.*,

116   2017) (Fig. 1A). Initially cells were imaged by dual-color SIM, which has a

117   resolution of ~ 100 nm (Gustafsson, 2000). This approach allowed us to

118   obtain an unhindered view of the divisome along the longitudinal axis of the

119   cell, without the need for 3D reconstructions from 2D images. For both FtsZ-

120   GFP and mCherry-FtsN we observed fluorescent rings (Fig. 1B). In cells

121   where the radius of the FtsZ-GFP was > 450 nm we observed that the radius

122   of the mCherry-FtsN signal appeared to be similar (Fig. 1B, left panel). We

123   reason that these cells had only just begun to constrict, as the radius of an

124   unconstricted cell is approximately 500 nm (Supporting Information Fig. S3).

125   For cells where the radius of FtsZ-GFP was < 450 nm we observed that the

126   radius of mCherry-FtsN was clearly larger (Fig. 1B, right panel). Identical

127   observations were obtained when we imaged cells co-expressing FtsZ-

128   mNeonGreen (-mNG) and mCherry-FtsN (Fig. 1C). Although FtsZ-mNG has a

129   mild GTPase phenotype (Yang *et al.*, 2017), it can be incorporated at the

130   native chromosomal locus and thus function as the only source of FtsZ in the

131   cell (Moore *et al.*, 2017). In our experiments we could confirm that FtsZ-mNG

132   was expressed at near native levels, and that it did not degrade (Supporting

133   Information Fig. S4). mCherry-FtsN was mildly expressed, at levels that were

134   less than two fold more than the wild type (Supporting Information Fig. S5).

135   To confirm that proteins in the Z-ring were separated from proteins in the PG

136   synthesizing machinery we imaged other proteins by dual-color SIM. When

137   we imaged ZipA-GFP (another marker for the Z-ring) and mCherry-FtsN we

138   observed that the radii of the fluorescence signals appeared to be similar

139   when the width of the cell was > 450 nm, but visibly separated when the width

140   was < 450 nm (Fig. 1D). A difference was not observed when imaging FtsZ-

141   mNG and FtsZ-mCherry, or ZipA-GFP and FtsZ-mCherry, (Supporting

142   Information Fig. S6). (Supporting Information Fig. S6). Similarly, the radii of

143   the fluorescence signals from GFP-FtsI (another marker for the PG

144   synthesizing machinery) and mCherry-FtsN remained similar throughout the

145   constriction process (Fig. 1E). These data are consistent with our previous

146   observations, which indicated that proteins in the Z-ring (i.e. FtsZ, FtsA, ZipA)

147   are radially separated from the PG synthesizing machinery (i.e. FtsQ, FtsL,

148   FtsI, FtsN) in constricting cells (Söderström *et al.*, 2016).

149   Analysis of the difference in peak-to-peak radii (Δr) of the protein pairs at

150   different stages of constriction suggested that the Z-ring was constricting

151   faster than the ring formed by the PG synthesizing machinery (Fig. 1F - G).

152   For example, the Δr between FtsZ and FtsN was 14.4 ± 9.7 nm at the onset of

153   constriction (r > 450 nm), 39.6 ± 4.5 nm in the middle of constriction (r ~ 450

154   nm to ~ 200 nm) and 45.8 ± 5.2 nm at a later stage of constriction (r < 200

155   nm) (Fig. 1H). When r < 100 nm, FtsZ disassembled whilst FtsN stayed until

156   the daughter cells separated (see (Söderström *et al.*, 2014)). Taken together,

157   these measurements indicate that the majority of molecules in the Z-ring

158   separate from the majority of molecules in the PG synthesizing machinery.

159   The separation occurs at the onset of constriction and becomes increasingly

160   larger as the envelope is constricted.

161

162   To visualize the separation in finer detail we used time-gated STimulated

163   Emission Depletion (gSTED) nanoscopy, which has a resolution capability of

164   ~ 35 - 40 nm (Vicidomini *et al.*, 2011, Vicidomini *et al.*, 2013). In our

165   experimental conditions and microscopy parameters the resolution was

166   estimated to be ~ 50 nm (Supporting Information Fig. S7). In this series of

167   experiments, we co-expressed FtsZ-mNG from the chromosome and

168   mStrawberry-FtsN from a plasmid and imaged their relative positions at the

169   division site in cells trapped in microholes. Thus FtsZ-mNG was the only

170 source of FtsZ, whilst both the native FtsN and mStrawberry-FtsN were

171 present. In the conditions used for the experiment, the expression of

172 mStrawberry-FtsN was less than two fold more than the wild type (Supporting

173 Information Fig. S5). Moreover the fusion could complement an FtsN depleted

174 strain (Supporting Information Fig. S12). Initially gSTED imaging was done

175 using both live and fixed cells. The dual-color gSTED images were similar

176 using both methods; they showed that FtsZ-mNG and mStrawberry-FtsN

177 appeared as spots that were localized around the divisome. However, to

178 avoid motion induced blurring and relative protein motion during image

179 acquisition, we opted to use fixed cells (Fig. 2A). Line scans along the

180 circumference of the division site revealed that the spots were separated by

181 stretches that were completely devoid of fluorescence (Fig. 2A).

182 Discontinuous rings have been noted previously (Strauss *et al.*, 2012, Holden

183 *et al.*, 2014, Coltharp *et al.*, 2016, Rowlett & Margolin, 2014).

184 Curiously, even though FtsZ-mNG and mStrawberry-FtsN formed

185 discontinuous rings with similar radii, the proteins did not always co-localize

186 (Fig. 2B). Imaging fluorescent mircobeads ruled out channel misalignment

187 (Supporting Information Fig. S8). We therefore conclude that the vast majority

188 of FtsZ-mNG and mStrawberry-FtsN molecules are spatially separated, even

189 at a very early stage of constriction. gSTED imaging of mStrawberry was

190 technically challenging, particularly in constricting cells (r < 450 nm).

191 Nevertheless, were we able to confirm that FtsZ-mNG and mStrawberry-FtsN

192 constricted into discontinuous rings with different radii (Fig. 2C - G). The Δr

193 was on average 48.2 ± 6.5 nm (n = 8), which is consistent with data obtained

194 using SIM.

195   Intriguingly, in some gSTED images we observed cells where the radii formed

196   by FtsZ-mNG and mStrawberry-FtsN appeared to overlap in some sections,

197   but not in other sections (Supporting Information Fig. S8). This observation

198   suggests that constriction by the Z-ring is asymmetric. Similar observations

199   have been made in other bacteria, although not *E. coli* (Yao *et al.*, 2017).

200   Taken together the dual color gSTED images enabled us to better resolve

201   localization of FtsZ and FtsN, and determine that the majority of molecules

202   are spatially separated.

203

204   *Hidden details of the divisome ultra-structure*

205   The gSTED images of FtsZ-mNG indicated that the densities were often

206   irregular. For example, while most densities were positioned along the

207   circumference of the division site (Fig. 2C, line 1), some appeared to be

208   oriented perpendicular to the circumference (Fig. 2C, line 2). To better

209   understand these fine details, we analyzed single color gSTED images of

210   cells expressing only FtsZ-mNG (Fig. 3A). Quantitative measurements

211   revealed an average width (along the long axis of the cell) of 109 ± 14 nm (n =

212   10), and an average radial thickness of 80 ± 2 nm (n = 50) (Supporting

213   Information Fig. S9). The average length of the FtsZ-mNG patches was 109 ±

214   4 nm (n = 158) (Fig. 3B, 3N), and the average ring coverage was 65 ± 12 %, n

215   = 48 (Fig. 3O). Curiously, about 3 % of these patches were arranged in

216   helical-like structures within the rings (Fig. 3C). To validate these

217   observations, we immuno-decorated the native FtsZ in wild type cells (Fig.

218   3D). The average width of the ring in wild type cells was 116 ± 19 nm (n = 11)

219   (Supporting Information Fig. S11), the radial thickness 79 ± 2 nm (n = 58), the

220   average length was 115 ± 6 (n = 102) (Fig. 3E - F, 3N) and the average ring

221   density was 53 ± 8 % (n = 48). These observations of the antibody labeled

222   FtsZ are consistent with values obtained from FtsZ-mNG. They are also

223   consistent with PALM images using FtsZ-FP fusions (Fu *et al.*, 2010, Coltharp

224   *et al.*, 2016) and *in vitro* reconstitution experiments (Huecas *et al.*, 2008,

225   Romberg *et al.*, 2001, Chen *et al.*, 2005). In wild type cells, we observed that

226   roughly 5 % of the native FtsZ patches oriented perpendicular (or nearly so) to

227   the tangent of the ring (Fig. 3F, line 1). This latter observation is consistent

228   with, although less pronounced than, anisotropy measurements on FtsZ

229   filaments (Si *et al.*, 2013). It could be caused by internal disorganization in the

230   Z-ring, or by the fact that the Z-ring follows local membrane deformations.

231

232   We also characterized the septal organization of FtsN at a nanometer scale,

233   as this had not been done previously. For these experiments, we analyzed

234   images of mCitrine-FtsN and antibody labeled FtsN, again using gSTED.

235   mCitrine is a yellow fluorescent protein that has superior STED properties

236   (Vicidomini *et al.*, 2011, Hein *et al.*, 2008), and it was therefore used instead

237   of mStrawberry. In the conditions used for the experiment, the expression of

238   mCitrine-FtsN was less than two fold more than the wild type (Supporting

239   Information Fig. S5). Moreover the fusion could complement an FtsN depleted

240   strain (Supporting Information Fig. S12). The average width of mCitrine-FtsN

241   at the septum (along the long axis) was 127 ± 8 nm (n = 8) (Supporting

242   Information Fig. S9), the radial filament thickness of the densities in the ring

243   was 101 ± 2 nm (n = 46) (Supporting Information Fig. S9), and the length of

244   the filaments was 106 ± 3 nm (n = 190) (Fig. 3G - H). The average ring

245 coverage was 79 ± 7 % (n = 51) (Fig. 3O). Densities of antibody labeled FtsN

246 were similar to those observed from mCitrine-FtsN, ruling out artifacts caused

247 by mild overexpression or the use of tags. The average width of antibody

248 labeled FtsN was 126 ± 9 nm (n = 9) (Supporting Information Fig. S13), the

249 radial filament thickness 102 ± 2 nm (n = 39) and length 117 ± 3 nm (n = 182)

250 (Fig. 3K - M). The ring coverage was 81 ± 4 % (n = 26) (Fig. 3O). Although the

251 dimensions of FtsN densities were comparable to those formed by FtsZ, they

252 occupied approximately 20 % more area at the division site.

253 Taken together the single color gSTED images allowed us to quantify the

254 dimensions of individual densities of FtsZ and FtsN on a nanometer scale.

255 The subsequent analyses revealed that both FtsZ and FtsN are in large

256 protein assemblies (larger than the resolution achievable in our gSTED).

257 Since our previous data had established that these densities are spatially

258 separated, we reason that there are at least two types of large assemblies (or

259 polymers) present at the septum; one containing FtsZ and the other

260 containing FtsN

261

262 *Movement of the Z-ring and the proteins involved in PG synthesis around the*

263 *division site is not affected by separation*

264 Our observation that FtsZ and FtsN are radially separated during constriction

265 raises an interesting question; does the PG synthesizing machinery continue

266 to move around the septum even after separation from the Z-ring? To monitor

267 the movement of proteins we performed time-lapse SIM imaging on cells

268 simultaneously expressing a chromosomal FtsZ-GFP fusion and mCherry-

269 FtsN expressed from a plasmid. We observed that the fluorescence densities

270   did indeed move around the circumference of the division site (Fig. 4A;

271   Supporting Movie S1), and that these movements were maintained even

272   when the radius of FtsZ-GFP was clearly smaller than that of mCherry-FtsN

273   (Fig. 4B; Supporting Movie S2). Analogous observations were made in cells

274   co-expressing ZipA-GFP and mCherry-FtsN, confirming that the separation

275   does not limit FtsN movement (Supporting Movies S3 and S4). Although, the

276   time resolution in our SIM system was not adequate to accurately determine

277   the velocity of the moving clusters, kymographs obtained from epi-

278   fluorescence time-lapse images using a higher time resolution (2 sec / image)

279   gave an estimated velocity for FtsZ and ZipA of 29 ± 5 nm/sec (n = 23) and 23

280   ± 11 nm/sec (n = 9), respectively (Supporting Information Fig. S14). Due to

281   the fact that the mCherry-FtsN assemblies were more confluent within the

282   rings, we were unable to extract a reliable estimation of their velocity

283   (Supporting Information Fig. S14). Nevertheless, our observations indicate

284   that both FtsZ and FtsN move around the circumference of the septum, even

285   when the radii of the respective rings are separated by as much as 50 nm.

286   This observation is consistent with recent literature, which noted that the Z-

287   ring (specifically FtsZ and FtsA) and proteins involved in PG synthesis

288   (specifically FtsI) traverse the circumference of the septum (Yang *et al*., 2017,

289   Bisson-Filho *et al*., 2017). We must stress though, that our data do not

290   provide any indication as to whether FtsZ treadmilling is physically driving the

291   circular motion of proteins involved in PG synthesis. Although this scenario

292   seems unlikely, given the spatial separation we have observed, it is formally

293   possible. For example, if another protein or proteins was physically linking

294 FtsZ to the proteins involved in PG synthesis. Or if there were small

295 populations of FtsZ and FtsN, that eluded detection in our experiments.

296

297 *Movement of the FtsZ and FtsN is mechanistically different*

298 To better understand the underlying mechanism(s) by which FtsZ and FtsN

299 exchange protein subunits at the division site, we monitored their respective

300 dynamics using confocal Fluorescence Recovery After Photobleaching

301 (FRAP). In these experiments, we trapped live cells co-expressing FtsZ-GFP

302 and mCherry-FtsN in microholes, then photobleached sections of their

303 respective rings and monitored the recovery of the signal. Fig. 5A shows an

304 example where a quarter of a ring was bleached and the subsequent recovery

305 monitored over time. This experiment allowed us to determine how fast

306 fluorescent molecules re-enter the bleached areas of the rings, which gives an

307 indication of their exchange rate. When quarter rings were bleached, we

308 observed that the average $t_{1/2}$ of FtsZ-GFP was 3.92 ± 0.21 s and that of

309 mCherry-FtsN was 0.80 ± 0.34 s (n = 9) (Fig. 5B).

310 When half rings were bleached, we observed that the $t_{1/2}$ increased

311 proportionally, as expected for a larger area. For example, FtsZ-mNG (8.45 ±

312 2.21 s, n = 8), FtsZ-GFP (9.87 ± 2.52 s, n = 7), mCherry-FtsN (1.43 ± 0.52 s,

313 n = 6) or mCitrine-FtsN (1.87 ± 0.66 s, n = 9) (Fig. 5C and Supporting

314 Information Fig. S15). As expected, the fluorescence recovery was dependent

315 on the diffusion of proteins in the cell, as we did not observe it when cells

316 were fixed (Supporting Information Fig. S15). These FRAP data on FtsZ are in

317 good agreement with published data, obtained from cells lying flat on agarose

318 pads (9 ± 3 s, (Anderson *et al.*, 2004)). The ~ 4-5-fold faster recovery times

13

319 observed for FtsN compared to FtsZ indicate that the rate at which FtsN

320 subunits are exchanged at the septum is faster than the rate at which FtsZ

321 treadmills. The difference in recovery rate was not an artifact of the

322 fluorophores, as we had used two different fluorophores for both FtsZ and

323 FtsN.

324 In a separate series of FRAP experiments, we bleached all molecules except

325 those in the top and bottom of the rings and monitored the re-appearance of

326 fluorescence molecules (Fig. 5D - E). We observed that FtsZ-GFP

327 fluorescence reappeared at different places throughout the bleached regions

328 of the ring (Fig. 5D, white arrows; Supporting Movie S5). The same behavior

329 was observed when monitoring the fluorescence recovery in cells expressing

330 FtsZ-mNG (Fig. 5E). These data are consistent with polymer rebuilding *in*

331 *vivo*, and they validate previous TIRF data that show FtsZ treadmilling *in vitro*

332 and *in vivo* (Yang et al., 2017, Loose & Mitchison, 2014, Bisson-Filho et al.,

333 2017).

334 Photobleaching large sections of the rings formed by FtsN was not feasible,

335 since there are generally fewer proteins present in the cell. We therefore

336 bleached half of the ring and followed the redistribution of fluorescence at a

337 higher time resolution. Curiously, recovery of FtsN was always evenly

338 distributed over the bleached area (Fig. 5F). Although we still do not fully

339 understand what underlying mechanism drives subunit exchange in the PG

340 synthesizing machinery, our data does suggest that it is different to FtsZ. FtsN

341 subunits exchange continuously, not constrained by polarity, while on the

342 other hand FtsZ monomers are added directionally and recovery behavior is

343 therefore consistent with treadmilling motion.

344

345

346   **Discussion**

347   The division of an *E. coli* cell requires the coordinated action of at least thirty-

348   four different proteins (Haeusser & Margolin, 2016, de Boer, 2010). It has

349   been largely assumed that these proteins assemble into a single

350   macromolecular complex. However, recent data from our labs suggested that,

351   during constriction of the cell envelope, proteins in the Z-ring (FtsZ, FtsA,

352   ZipA) were largely separated from proteins required for PG synthesis (FtsQ,

353   FtsL, FtsI, FtsN) (Söderström & Daley, 2017, Söderström *et al.*, 2016). The

354   separation of these different proteins into functional modules has important

355   implications for understanding how the divisome proteins coordinate

356   constriction of the cell envelope, so we were motivated to better understand

357   the separation. Herein, our experiments focused on FtsZ and FtsN as they

358   represent the Z-ring and the PG synthesizing machinery respectively. The

359   approach we took was to co-express FtsZ and FtsN as FP fusions, then

360   immobilize cells in a 'standing' position and image them using either dual-

361   color SIM (live cells) or gSTED (fixed cells). gSTED images indicated that

362   both proteins appeared as discrete densities that were organized as

363   discontinuous rings around the septum. The dimensions of the densities were

364   consistent with either large protein assemblies or filaments and bundles. A

365   back of the envelope calculation based on the dimensions of the densities and

366   the average ring coverage, indicates that there are between 13 and 18 visible

367   FtsZ densities in an unconstricted cell. For FtsN we calculated 21 - 22

368   densities per unconstricted cell. Thus, there are fewer FtsZ densities in the

369 cell. The discontinuous rings we observed when imaging FtsZ are consistent

370 with a number of previous studies that have used fluorescence microscopy

371 (Rowlett & Margolin, 2014, Holden *et al.*, 2014, Strauss *et al.*, 2012, Fu *et al.*,

372 2010, Coltharp *et al.*, 2016, Jacq *et al.*, 2015). However, it should be noted

373 that cryo-ET imaging has shown that FtsZ protofilaments can form both

374 continuous ribbons around the division septum as well as largely

375 discontinuous Z-rings (Szwedziak *et al.*, 2014, Yao *et al.*, 2017).

376 Significantly, our images indicated that the bulk of the FtsZ and FtsN

377 fluorescence emission was spatially separated during constriction. At an early

378 stage of constriction (r > 450 nm), we observed that the assemblies containing

379 FtsZ and FtsN were distributed around the division site with a similar radius,

380 but they did not always overlap. Once the cells started to visibly constrict (r <

381 450 nm), the radius of the ring formed by the FtsZ containing complexes was

382 approximately 50 nm smaller than that of the ring formed by the FtsN

383 containing complexes. Quantitative analysis of the SIM images indicated that

384 the difference between the radii gradually increased as constriction

385 progressed. The radial separation cannot be explained by topological

386 differences between the FP moieties that were fused to FtsZ and FtsN, as

387 these moieties were both localized to the cytoplasm and should be close to

388 the inner membrane. Moreover, it cannot be explained by extension of the

389 unstructured linker that separates FtsZ from its C-terminal anchor, as this

390 linker is only 17 nm long in its fully extended conformation (Erickson *et al.*,

391 2010, Ohashi *et al.*, 2007). We believe that the most likely interpretation of

392 these data is that the majority of FtsZ molecules are physically separated from

393 the majority of the FtsN molecules. Considering that electron microscopy

394   images of dividing cells have indicated that the septal invagination is steep

395   (see (Burdett & Murray, 1974a, Burdett & Murray, 1974b)), we reason that the

396   majority of FtsZ molecules are localized at the leading edge of the

397   invagination, whereas the majority of FtsN molecules are localized

398   approximately 50 nm further back from the leading edge (Fig. 6).

399   We also explored the mechanism(s) of FtsZ and FtsN movement around the

400   septum using a photobleaching assay. We observed that following bleaching,

401   FtsZ recovered 4-5 times slower than FtsN. We also observed that FtsZ

402   recovered as continuously and directionally growing polymers that were

403   consistent with filament treadmilling behavior, whilst FtsN recovered in a

404   fundamentally different manner. Taken together the data suggest that both

405   FtsZ and FtsN clusters do traverse the septum, but that the majority of

406   molecules do so within radially separated densities using different

407   mechanisms.

408   The spatial separation of FtsZ and FtsN raises a simple but as of yet

409   unresolved question; what is the divisome? For some time, the divisome has

410   been considered as a large protein complex containing all divisome proteins.

411   This may very well be true at an early time point in the assembly process,

412   which we were not able to capture in our images; we assume that constriction

413   was initiated in our experiments since FtsN was localized to the septum

414   (Weiss, 2015). It may also be true if there is a small population of FtsZ or FtsN

415   that has evaded detection. Or alternatively, if FtsZ and FtsN are connected by

416   other divisome proteins. For example, FtsA is known to physically interact with

417   both FtsZ and FtsN, and in theory, it could act as a bridge between the two.

418   However, we believe our data point to the existence of spatially separated

419   protein complexes.

420   The existence of spatially separated assemblies that contain either FtsZ or

421   FtsN at the septum is broadly consistent with what is known about the arrival

422   of proteins at the division site. Specifically, that those proteins in the Z-ring

423   arrive at the septum first, forming a scaffold that recruits proteins required for

424   PG synthesis (Aarsman *et al.*, 2005). That FtsZ and FtsN are organized in

425   different complexes is also consistent with studies timing the departure of

426   proteins from the septum, which have shown that FtsZ and other proteins in

427   the Z-ring move away from the septum prior to proteins required for PG

428   synthesis (Söderström *et al.*, 2016, Söderström *et al.*, 2014). If the Z-ring and

429   the proteins involved in PG synthesis were part of a single macromolecular

430   complex, one could expect that disassembly of the scaffold would also

431   release the proteins involved in PG synthesis. But this is not the case.

432   The radial separation, combined with differences in ring densities of FtsZ and

433   FtsN has important implications for understanding how envelope constriction

434   is coordinated. It has been recently demonstrated that treadmilling of FtsZ

435   modulates the directional movements of FtsI (although FtsZ and FtsI did not

436   appear to have the same average circumferential velocity), and from this data

437   it was hypothesized that PG in-growth is stimulated at sites where FtsZ

438   polymers are constricting (Yang *et al.*, 2017, Bisson-Filho *et al.*, 2017).

439   However, it remains to be determined how FtsZ polymers can 'control' the

440   localization of the proteins involved in PG synthesis (see (Schoenemann &

441   Margolin, 2017, Du & Lutkenhaus, 2017, Coltharp & Xiao, 2017)). A physical

442   coupling has been implied (Schoenemann & Margolin, 2017), and this maybe

443   the case, if there are small populations of molecules that have either evaded

444   detection in our studies. Or, if molecules on the fringes of the fluorescent

445   signals are physically interacting. However, given the spatial separation

446   during constriction, combined with differences in ring coverage and the

447   temporal differences in departure from the septum, this scenario is difficult to

448   envision.

449

450   **Experimental Procedures**

451

452   *Plasmids*

453   Generation of fluorescent fusion proteins was performed using the Gibson

454   assembly protocol (Gibson *et al.*, 2009) with Q5-polymerase (NEB) used as a

455   replacement to Phusion-polymerase. Plasmids created for this study

456   (pPS001, pHC002 and pHC004) contain a pRha67 backbone, which has a

457   high-copy pUC origin of replication (Giacalone *et al.*, 2006). In the version of

458   pRha67 that we used, the original ampicillin resistance marker was replaced

459   with a kanamycin resistance marker (Hjelm *et al.*, 2015). All plasmids are

460   listed in Supporting Information Table S1. The coding sequence for FtsZ was

461   sourced from the K12-derived strain MC1061, while codon optimized

462   mTagBFP, mStrawberry, and mCitrine were sourced from Genscript, Clontech

463   and the mCitrine-N1 plasmid respectively. PCR of each fluorescent target and

464   the respective rhamnose-inducible pRha67 plasmid (Giacalone *et al.*, 2006,

465   Söderström *et al.*, 2016) was performed using primers listed in Supporting

466   Information Table S2. The FtsZ-mTagBFP contains a linker sequence

467   encoding NNNLQ, between FtsZ and mTagBFP. The mStrawberry-FtsN and

468   mCitrine-FtsN contain a linker sequence encoding ASEL, between the

469   fluorescent protein and the respective divisome protein. All plasmid

470   sequences were verified by DNA sequencing (Eurofins MWG or Fasmac,

471   Japan).

472

473   *Bacterial growth*

474   Pre-cultures of were grown overnight in 20 ml of LB with appropriate

475   antibiotics (Kanamycin 50 µg ml^{-1}, Ampicillin 50 µg ml^{-1}, Chloramphenicol 15

476   µg ml^{-1}, Spectinomycin 30 µg ml^{-1}) at 37 °C. The following morning the

477   cultures were back-diluted 1:50 in LB, and incubated at 30 °C or 37 °C to

478   OD$_{600}$ 0.2-0.5. Strains expressing FtsZ-mNG were grown in M9 minimal

479   media supplemented with 1µg ml^{-1} thiamine, 0.2 % (w/v) glucose and 0.1 %

480   (w/v) casamino acids appropriate antibiotics when needed (Kanamycin 50 µg

481   ml^{-1}, Ampicillin 50 µg ml^{-1}, Chloramphenicol 15 µg ml^{-1}, Spectinomycin 30 µg

482   ml^{-1}), and incubated at 30 °C OD$_{600}$ 0.2-0.5. For a complete list of strains and

483   plasmids used in the work see Supporting Information Table S1.

484

485   *Fluorescent protein production*

486   Chromosomally encoded FtsZ-mNeonGreen was integrated at the native *ftsZ*

487   locus and needed no inducer (Moore *et al.*, 2017). Chromosomally encoded

488   FtsZ-GFP, ZipA-GFP and GFP-FtsI were induced by 2.5, 50, 5 µM IPTG,

489   respectively (Söderström *et al.*, 2016, Söderström *et al.*, 2014). Plasmid

490   encoded FtsZ-mTagBFP was induced by 5 mM rhamnose. Plasmid encoded

491   mCherry-FtsN, mStrawberry-FtsN and Citrine-FtsN were induced by either 2.5

492   or 5 mM rhamnose. FtsZ-mCherry was induced with 0.2 % arabinose, as

493   described previously (Galli & Gerdes, 2010). Expression levels of fusion

494   proteins relative to the native protein, was assessed by Western blotting

495   (Supporting Information Fig. S4 and S11).

496

497   *Nanofabrication of the micropillar mold*

498   The approach for the micron-sized pillars was adapted from (Bisson-Filho et

499   al., 2017). Micron-scale pillars were fabricated on a Silicon (Si) substrate by

500   reactive ion etching, using a multi-step process similar to the one described in

501   (Antonov *et al.*, 2015). Briefly, a pattern of hard-baked photoresist was

502   created on a Si surface using UV lithography, to work as a mask for etching.

503   The etching was performed using an Oxford Plasmalab100 ICP180 CVD/Etch

504   system, with a mixture of SF_6 and O_2 plasma as an etchant. Increasing

505   concentration of O_2 in the mixture has two effects: (i) it improves etching

506   anisotropy, which is essential for pillar formation; (ii) it reduces Si to

507   photoresist selectivity ratio, which limits the possible height of pillars. For our

508   process the ratio of $SF_6:O_2$ = 1:1 was optimal. After the etching, the remaining

509   photoresist was removed by O_2 plasma treatment. Pillar arrays (1 x 1 cm or 2

510   x 2 cm) were made with one micron sized pillar every 5 micrometers, with

511   dimensions between 1.1 and 1.4 microns wide and 4.5 - 6 microns high.

512

513   *Production of microholes in agarose beds*

514   Agarose (2.5-5% w/v) was dispersed on glass slides and the silica mold was

515   placed on top. Once the agarose had solidified the mold was removed and ~

516   10 μl of live cell culture (at OD_{600} 0.2-0.5 concentrated 10x by centrifugation)

517   was applied, incubated for ~ 1 minute whereby the excess liquid was removed

518 and the agarose pad covered with a pre-cleaned cover glass (#1.5). In order

519 to minimize the risk of motion blurring during image acquisition, each cell was

520 initially monitored using bright field and Epi/confocal fluorescence illumination

521 to verify that no visible movements were observed.

522

523 *Cell fixation, immunofluorescence and WGA labeling*

524 Cells were fixed and immunodecorated as described previously (Ogino *et al.*,

525 2004, Söderström *et al.*, 2016), with minor adjustments as follows. Briefly, 900

526 μl of ice-cold methanol was added to 100 μl of cell culture (OD$_{600}$ ~0.2 – 0.5)

527 and incubated for 5 minutes on ice. Cells were harvested by centrifugation

528 and resuspended in 100 μl of 90 % (v/v) ice-cold methanol. For

529 immunodecoration of cells, roughly 20 μl of cell suspension applied on a cover

530 glass coated with Poly-L-Lysine or on agarose microhole beds and left for ~ 2

531 minutes before excess culture was removed. After drying, the cells were

532 treated with lysozyme solution (0.2 mg/mL lysozyme, 25 mM Tris-HCl pH 8.0,

533 50 mM glucose, 10 mM EDTA) for 5 min and then rinsed with PBSTS

534 [140 mM NaCl, 2 mM KCl, 8 mM Na$_2$HPO$_4$, 0.05% (v/v) Tween 20, 20% (w/v)

535 sucrose], before they were treated with methanol for 1 min and acetone for

536 1 min and dried. Fixed cells were incubated with 2% (w/v) bovine serum

537 albumin in PBSTS for at least 15 min. Thereafter the cells were washed with

538 PBSTS and incubated with primary antibodies against FtsZ (Rabbit, Agrisera,

539 Sweden) or FtsN (Rabbit, (Wissel & Weiss, 2004)) diluted 1:200 in the same

540 buffer for at least 1 hour at RT, or overnight at 4 °C. Oregon Green 488-

541 conjugated anti-rabbit serum (Molecular Probes) at a 1:500 dilution (in PBSTS

542 containing 2 % (w/v) BSA) was used as secondary antibody against FtsZ due

543   to its STED compatibility. Between each incubation, and after the last, the

544   cells were washed at least 10 times in PBSTS. Cells on cover glasses were

545   placed on glass slides with ~ 20 μl Moviol as mounting media and left

546   overnight to harden before imaging, while cells in agarose microhole beds

547   were covered with a pre-cleaned cover glass (♯1.5) and imaged directly.

548   For cell width determination of unconstricted cells, WGA (Wheat Germ

549   Agglutinin) conjugated with Oregon Green 488 (f.c. 100 μm ml^{-1}) was applied

550   to exponentially growing cells, cultures were allowed to grow for ~ 3 hours,

551   and then fixed in either 2 % PFA (15 minutes in RT) or 90 % ice-cold

552   methanol (5 minutes on ice). After fixation the cultures were washed 2 times

553   in PBS and directly applied to an agarose pad before imaging.

554

555   *Imaging on flat agarose beds or in microholes*

556   Gated STED (gSTED) images were acquired on a Leica TCS SP8 STED 3X

557   system, using a HC PL Apo 100x oil immersion objective with NA 1.40.

558   Fluorophores were excited using a white excitation laser operated at 488 nm

559   (for mNeonGreen and OG488) or 506 nm (for mCitrine), a STED laser line

560   operated at 592 nm, and detection time-delay of 0.9 - 2.5 ns. mStrawberry

561   was excited using a 574 nm laser light and depleted using a 660 nm STED

562   laser line, and the delay-time was 0.5-0.8 ns. The total depletion laser

563   intensity was on the order of 20-100 MW/cm^2 for all experiments. The final

564   pixel size was 13 nm and scanning speed 600 Hz. The pinhole size was

565   varied between 0.4-0.9 AU; a smaller pin-hole when imaging cells standing

566   trapped in microholes and larger when imaging cells laying flat on agarose

567   pads.

568   Epi-fluorescence, confocal and SIM images were acquired on either a Zeiss

569   LSM780 or Zeiss ELYRA PS1 (both equipped with a 100X 1.46NA plan Apo

570   oil immersion objective) with acquisition times between 0.3 and 2 sec. Time-

571   lapse movies were recorded with intervals of 1 - 10 seconds. SIM images

572   were acquired using ELYRA PS1 (pco.edge sCMOS camera). Pixel size 50

573   nm in SIM images. SIM time-lapse movies (containing either 7 or 10 frames)

574   were recorded with time intervals between 0 sec and 5 minutes. Individual

575   images were acquired with acquisition times between 300 and 500 ms per

576   image (a total of 15 images were acquired per SIM image reconstruction) and

577   subsequently reconstructed from the raw data in the ZEN2012 software. It is

578   important to note that images in different channels in the SIM time-lapse

579   images were acquired sequentially (total acquisition time for one channel was

580   between ~ 7 - 10 seconds), thus the relative density (protein) localization

581   within the rings cannot be analyzed in this way, only the relative radial

582   overlap/separation between respectively channel can be assessed. All

583   imaging was performed at room temperature (~23-24 °C).

584

585   *Image analysis*

586   STED images were deconvolved using Huygens Professional deconvolution

587   software (SVI, the Netherlands). Epi-fluorescence and SIM image stacks were

588   drift-corrected using the ImageJ plugin StackReg. Images were background

589   subtracted using a rolling ball radius of 50. To determine the difference in radii

590   between the Z-ring proteins and FtsN in Fig. 1, we assumed the cells to have

591   a circular shape and line scans were drawn from 3 o'clock to 9 o'clock over

592   the rings. The resulting peak-to-peak distance was analyzed in Origin9 Pro.

593   The two fluorescence maxima were fitted to Gaussians using the multiple

594   peak analyzer function in Origin9 Pro, and from the fitted maxima the

595   diameter was subsequently extracted. The respective ring radii were then

596   calculated and the smaller (e.g. FtsZ) was subtracted from the larger (i.e.

597   FtsN) in order to determine the difference in radii, Δr.

598   For cells imaged by gSTED the radii were estimated from a circle drawn along

599   the maxima of the fluorescence profiles. Cluster length and width values were

600   obtained from the entire population of cells using line scans (line size 3) over

601   randomly selected individual protein clusters (2-4 clusters per cell) from

602   deconvolved images. A Gaussian distribution was fitted to the intensity

603   profiles in order to extract the Full Width at Half Maximum (FWHM). The

604   resolution in our gSTED images was ~ 50 nm (Supporting Information Fig.

605   S7). Clusters did not always follow the circumference of the cells therefore we

606   always regarded the long axis as "length" and the short axis as "width".

607   Kymographs were generated using the ImageJ plugin KymoResliceWide

608   applied on lines drawn long the circumference of the cells (fluorescence

609   profile). The mean velocity was subsequently extracted manually by following

610   individual filaments bundles over time and then converting the traveled

611   distance from degrees to nm, as described (Loose & Mitchison, 2014). The

612   ring coverage was estimated from line scans with lines thicker than the

613   fluorescence signal in the radial direction. The portion of the circumference,

614   normalized to length, which had none-zero intensity, was integrated to obtain

615   the ring coverage in % of total ring length. Note that ~ 10 % of the normalized

616   signal was subtracted as background, thus the presented absolute values of

617   ring coverage may be slightly underestimated.

618

619   *FRAP analysis*

620   Confocal FRAP measurements were performed on a Zeiss LSM780 system,

621   using a 100x 1.4NA plan Apo oil immersion objective and pinhole size of

622   varying between 60 and 20 µm. Bleaching was performed using 100% laser

623   power applied over the region of interest between 0.4 and 1 second, and data

624   was collected in time intervals between 0.6 and 10 seconds. After background

625   correction, the fluorescence intensity of the bleached region (half a ring,

626   quarter of a ring or other) was normalized to the average ring fluorescence of

627   an area of same size as the bleached; $F_{NORM}(t) = F_{BLEACHED}(t)/(F_{BLEACHED}(t)+$

628     $_{UNBLEACHED}(t))$. All data was exported to Origin9 Pro and data points were fitted

629   to the single exponential function $F(t) = F_{end} - (F_{end} - F_{start})* e^{-kt}$, where $F(t)$ is

630   the fluorescence intensity at time t, F_{end} is the fluorescence intensity at

631   maximum recovery, F_{start} is the fluorescence recovery momentarily after

632   bleaching (at t = 0), and k is a free parameter. The recovery half time was

633   then extracted from $t_{1/2}$ = ln 2 / k. Importantly, all cells were scanned from top

634   to bottom in order to find the division plane (in which the rings reside).

635   *Cell length and width measurements*

636   Cells from 1 ml cultures were harvested by centrifugation. The cultures were

637   washed twice in 200 µl PBS before an aliquot (~ 6 µl) was placed on an

638   agarose bed and directly imaged under bright-field illumination. Cell lengths of

639   at least 100 cells from each strain were determined using the ROI manager in

640   ImageJ and statistics were calculated and graphs were produced using

641   OriginPro9.

642

643   *Cryo-electron microscopy*

644   WT cells were grown as described above. A 2 μl aliquot of cell culture was

645   applied on glow discharged EM grids (Quantifoil, 3,5/1, Cu 200 mesh) and

646   directly flash frozen in liquid Ethane using a FEI Vitrobot. Subsequent imaging

647   was performed on an FEI Titan KRIOS 300 kVe electron microscope, using a

648   nominal magnification of 22500X. Image acquisition time was 1 second, the

649   underfocus was kept at − 8 μm. Images were resolution and contrast

650   enhanced using the COMET (Skoglund *et al.*, 1996) software operated in 2D

651   mode.

652

653   *Western blotting*

654   Cell extracts from a volume corresponding to 0.1 DO_{600} units were collected

655   for different strains. The extracts were suspended in loading buffer and

656   resolved by sodium dodecyl sulphatepolyacrylamide gel electrophoresis.

657   Proteins were transferred to nitrocellulose membranes using a semi-dry

658   Transfer-Blot apparatus (Bio-Rad). The membranes were blocked in 5 % (w/v)

659   milk and probed with antisera to either FtsZ (Agrisera, Sweden), FtsN (Wissel

660   & Weiss, 2004) or GFP (Abcam, UK).

670

671 **Conflict of interest**

672 The Authors declare no conflicts of interest.

673

674 **Author contributions**

675 B.S and D.O.D. designed the study and conceived the experiments. H.C and

676 P.S. contributed new reagents. B.S. performed the experiments. All authors

677 analysed the data. B.S and D.O.D. wrote the manuscript with input from the

678 other authors. All authors have read and approved the final version.

679

References

Aarsman, M.E., A. Piette, C. Fraipont, T.M. Vinkenvleugel, M. Nguyen-
    Disteche & T. den Blaauwen, (2005) Maturation of the *Escherichia coli*
    divisome occurs in two steps. *Molecular microbiology* **55**: 1631-1645.

Alexeeva, S., T.W. Gadella, Jr., J. Verheul, G.S. Verhoeven & T. den
    Blaauwen, (2010) Direct interactions of early and late assembling
    division proteins in *Escherichia coli* cells resolved by FRET. *Molecular*
    microbiology **77**: 384-398.

Anderson, D.E., F.J. Gueiros-Filho & H.P. Erickson, (2004) Assembly
    dynamics of FtsZ rings in *Bacillus subtilis* and *Escherichia coli* and
    effects of FtsZ-regulating proteins. *Journal of bacteriology* **186**: 5775-
    5781.

Antonov, P.V., M.R. Zuiddam & J.W.M. Frenken, (2015) Fabrication of high-
    aspect ratio silicon nanopillars for tribological experiments. *J Micro-
    Nanolith Mem* **14**.

Bisson-Filho, A.W., Y.P. Hsu, G.R. Squyres, E. Kuru, F. Wu, C. Jukes, Y.
    Sun, C. Dekker, S. Holden, M.S. VanNieuwenhze, Y.V. Brun & E.C.
    Garner, (2017) Treadmilling by FtsZ filaments drives peptidoglycan
    synthesis and bacterial cell division. *Science* **355**: 739-743.

Buddelmeijer, N. & J. Beckwith, (2004) A complex of the *Escherichia coli* cell
    division proteins FtsL, FtsB and FtsQ forms independently of its
    localization to the septal region. *Molecular microbiology* **52**: 1315-1327.

Burdett, I.D. & R.G. Murray, (1974a) Electron microscope study of septum
    formation in *Escherichia coli* strains B and B-r during synchronous
    growth. *Journal of bacteriology* **119**: 1039-1056.

705 Burdett, I.D. & R.G. Murray, (1974b) Septum formation in *Escherichia coli*:

706   characterization of septal structure and the effects of antibiotics on cell

707   division. *Journal of bacteriology* **119**: 303-324.

708 Buss, J., C. Coltharp, G. Shtengel, X. Yang, H. Hess & J. Xiao, (2015) A

709   multi-layered protein network stabilizes the *Escherichia coli* FtsZ-ring

710   and modulates constriction dynamics. *PLoS genetics* **11**: e1005128.

711 Chen, Y., K. Bjornson, S.D. Redick & H.P. Erickson, (2005) A rapid

712   fluorescence assay for FtsZ assembly indicates cooperative assembly

713   with a dimer nucleus. *Biophysical journal* **88**: 505-514.

714 Coltharp, C., J. Buss, T.M. Plumer & J. Xiao, (2016) Defining the rate-limiting

715   processes of bacterial cytokinesis. *Proceedings of the National*

716   *Academy of Sciences of the United States of America* **113**: E1044-

717   1053.

718 Coltharp, C. & J. Xiao, (2017) Beyond force generation: Why is a dynamic ring

719   of FtsZ polymers essential for bacterial cytokinesis? *BioEssays : news*

720   *and reviews in molecular, cellular and developmental biology* **39**: 1-11.

721 Daley, D.O., U. Skoglund & B. Soderstrom, (2016) FtsZ does not initiate

722   membrane constriction at the onset of division. *Scientific reports* **6**:

723   33138.

724 de Boer, P.A., (2010) Advances in understanding *E. coli* cell fission. *Curr Opin*

725   *Microbiol* **13**: 730-737.

726 den Blaauwen, T., L.W. Hamoen & P.A. Levin, (2017) The divisome at 25: the

727   road ahead. *Curr Opin Microbiol* **36**: 85-94.

728 Di Lallo, G., M. Fagioli, D. Barionovi, P. Ghelardini & L. Paolozzi, (2003) Use

729   of a two-hybrid assay to study the assembly of a complex

730   multicomponent protein machinery: bacterial septosome differentiation.

731   *Microbiol-Sgm* **149**: 3353-3359.

732   Du, S. & J. Lutkenhaus, (2017) Assembly and Activation of the *Escherichia*

733   *coli* Divisome. *Molecular microbiology*.

734   Egan, A.J. & W. Vollmer, (2013) The physiology of bacterial cell division.

735   *Annals of the New York Academy of Sciences* **1277**: 8-28.

736   Erickson, H.P., D.E. Anderson & M. Osawa, (2010) FtsZ in bacterial

737   cytokinesis: cytoskeleton and force generator all in one. *Microbiol Mol*

738   *Biol Rev* **74**: 504-528.

739   Fraipont, C., S. Alexeeva, B. Wolf, R. van der Ploeg, M. Schloesser, T. den

740   Blaauwen & M. Nguyen-Disteche, (2011) The integral membrane FtsW

741   protein and peptidoglycan synthase PBP3 form a subcomplex in

742   *Escherichia coli*. *Microbiol-Sgm* **157**: 251-259.

743   Fu, G., T. Huang, J. Buss, C. Coltharp, Z. Hensel & J. Xiao, (2010) In vivo

744   structure of the E. coli FtsZ-ring revealed by photoactivated localization

745   microscopy (PALM). *PLoS One* **5**: e12682.

746   Galli, E. & K. Gerdes, (2010) Spatial resolution of two bacterial cell division

747   proteins: ZapA recruits ZapB to the inner face of the Z-ring. *Molecular*

748   *microbiology* **76**: 1514-1526.

749   Gerding, M.A., B. Liu, F.O. Bendezu, C.A. Hale, T.G. Bernhardt & P.A. de

750   Boer, (2009) Self-enhanced accumulation of FtsN at Division Sites and

751   Roles for Other Proteins with a SPOR domain (DamX, DedD, and

752   RlpA) in *Escherichia coli* cell constriction. *Journal of bacteriology* **191**:

753   7383-7401.

754   Giacalone, M.J., A.M. Gentile, B.T. Lovitt, N.L. Berkley, C.W. Gunderson &

755   M.W. Surber, (2006) Toxic protein expression in *Escherichia coli* using

756   a rhamnose-based tightly regulated and tunable promoter system.

757   *Biotechniques* **40**: 355-364.

758   Gibson, D.G., L. Young, R.Y. Chuang, J.C. Venter, C.A. Hutchison & H.O.

759   Smith, (2009) Enzymatic assembly of DNA molecules up to several

760   hundred kilobases. *Nature methods* **6**: 343-U341.

761   Goehring, N.W. & J. Beckwith, (2005) Diverse paths to midcell: assembly of

762   the bacterial cell division machinery. *Curr Biol* **15**: R514-526.

763   Gustafsson, M.G.L., (2000) Surpassing the lateral resolution limit by a factor

764   of two using structured illumination microscopy. *J Microsc-Oxford* **198**:

765   82-87.

766   Haeusser, D.P. & W. Margolin, (2016) Splitsville: structural and functional

767   insights into the dynamic bacterial Z ring. *Nat Rev Microbiol* **14**: 305-

768   319.

769   Hein, B., K.I. Willig & S.W. Hell, (2008) Stimulated emission depletion (STED)

770   nanoscopy of a fluorescent protein-labeled organelle inside a living cell.

771   *Proceedings of the National Academy of Sciences of the United States*

772   *of America* **105**: 14271-14276.

773   Hjelm, A., B. Soderstrom, D. Vikstrom, W.S. Jong, J. Luirink & J.W. de Gier,

774   (2015) Autotransporter-based antigen display in bacterial ghosts.

775   *Applied and environmental microbiology* **81**: 726-735.

776   Holden, S.J., T. Pengo, K.L. Meibom, C. Fernandez Fernandez, J. Collier & S.

777   Manley, (2014) High throughput 3D super-resolution microscopy

778   reveals *Caulobacter crescentus in vivo* Z-ring organization.

779   *Proceedings of the National Academy of Sciences of the United States*

780   *of America* **111**: 4566-4571.

781   Huecas, S., O. Llorca, J. Boskovic, J. Martin-Benito, J.M. Valpuesta & J.M.

782   Andreu, (2008) Energetics and geometry of FtsZ polymers: nucleated

783   self-assembly of single protofilaments. *Biophysical journal* **94**: 1796-

784   1806.

785   Jacq, M., V. Adam, D. Bourgeois, C. Moriscot, A.M. Di Guilmi, T. Vernet & C.

786   Morlot, (2015) Remodeling of the Z-Ring Nanostructure during the

787   Streptococcus pneumoniae Cell Cycle Revealed by Photoactivated

788   Localization Microscopy. *mBio* **6**.

789   Karimova, G., N. Dautin & D. Ladant, (2005) Interaction network among

790   *Escherichia coli* membrane proteins involved in cell division as

791   revealed by bacterial two-hybrid analysis. *Journal of bacteriology* **187**:

792   2233-2243.

793   Loose, M. & T.J. Mitchison, (2014) The bacterial cell division proteins FtsA

794   and FtsZ self-organize into dynamic cytoskeletal patterns. *Nature cell*

795   *biology* **16**: 38-46.

796   Meier, E.L. & E.D. Goley, (2014) Form and function of the bacterial cytokinetic

797   ring. *Current opinion in cell biology* **26**: 19-27.

798   Moore, D.A., Z.N. Whatley, C.P. Joshi, M. Osawa & H.P. Erickson, (2017)

799   Probing for Binding Regions of the FtsZ Protein Surface through Site-

800   Directed Insertions: Discovery of Fully Functional FtsZ-Fluorescent

801   Proteins. *Journal of bacteriology* **199**.

802   Muller, P., C. Ewers, U. Bertsche, M. Anstett, T. Kallis, E. Breukink, C.

803   Fraipont, M. Terrak, M. Nguyen-Disteche & W. Vollmer, (2007) The

804   essential cell division protein FtsN interacts with the murein

805   (peptidoglycan) synthase PBP1B in *Escherichia coli*. *Journal of*

806   *Biological Chemistry* **282**: 36394-36402.

807   Ogino, H., M. Wachi, A. Ishii, N. Iwai, T. Nishida, S. Yamada, K. Nagai & M.

808   Sugai, (2004) FtsZ-dependent localization of GroEL protein at possible

809   division sites. *Genes to cells : devoted to molecular & cellular*

810   *mechanisms* **9**: 765-771.

811   Ohashi, T., S.D. Galiacy, G. Briscoe & H.P. Erickson, (2007) An experimental

812   study of GFP-based FRET, with application to intrinsically unstructured

813   proteins. *Protein science : a publication of the Protein Society* **16**:

814   1429-1438.

815   Osawa, M., D.E. Anderson & H.P. Erickson, (2008) Reconstitution of

816   contractile FtsZ rings in liposomes. *Science* **320**: 792-794.

817   Osawa, M., D.E. Anderson & H.P. Erickson, (2009) Curved FtsZ

818   protofilaments generate bending forces on liposome membranes.

819   *EMBO J* **28**: 3476-3484.

820   Osawa, M. & H.P. Erickson, (2013) Liposome division by a simple bacterial

821   division machinery. *Proceedings of the National Academy of Sciences*

822   *of the United States of America* **110**: 11000-11004.

823   Pazos, M., P. Natale, W. Margolin & M. Vicente, (2013) Interactions among

824   the early *Escherichia coli* divisome proteins revealed by bimolecular

825   fluorescence complementation. *Environmental microbiology* **15**: 3282-

826   3291.

827   Romberg, L., M. Simon & H.P. Erickson, (2001) Polymerization of FtsZ, a

828   bacterial homolog of tubulin. is assembly cooperative? *J Biol Chem*

829   **276**: 11743-11753.

830   Rowlett, V.W. & W. Margolin, (2014) 3D-SIM super-resolution of FtsZ and its

831   membrane tethers in *Escherichia coli* cells. *Biophysical journal* **107**:

832   L17-20.

833   Rowlett, V.W. & W. Margolin, (2015) The bacterial divisome: ready for its

834   close-up. *Philosophical transactions of the Royal Society of London.*

835   *Series B, Biological sciences* **370**.

836   Schoenemann, K.M. & W. Margolin, (2017) Bacterial Division: FtsZ Treadmills

837   to Build a Beautiful Wall. *Curr Biol* **27**: R301-R303.

838   Si, F., K. Busiek, W. Margolin & S.X. Sun, (2013) Organization of FtsZ

839   filaments in the bacterial division ring measured from polarized

840   fluorescence microscopy. *Biophysical journal* **105**: 1976-1986.

841   Skoglund, U., L.G. Ofverstedt, R.M. Burnett & G. Bricogne, (1996) Maximum-

842   entropy three-dimensional reconstruction with deconvolution of the

843   contrast transfer function: a test application with adenovirus. *J Struct*

844   *Biol* **117**: 173-188.

845   Söderström, B. & D.O. Daley, (2017) The bacterial divisome: more than a

846   ring? *Current genetics* **63**: 161-164.

847   Söderström, B., K. Mirzadeh, S. Toddo, G. von Heijne, U. Skoglund & D.O.

848   Daley, (2016) Coordinated disassembly of the divisome complex in

849   *Escherichia coli*. *Molecular microbiology* **101**: 425-438.

850   Söderström, B., K. Skoog, H. Blom, D.S. Weiss, G. von Heijne & D.O. Daley,

851   (2014) Disassembly of the divisome in *Escherichia coli*: evidence that

852 FtsZ dissociates before compartmentalization. *Molecular microbiology*

853 **92**: 1-9.

854 Strauss, M.P., A.T.F. Liew, L. Turnbull, C.B. Whitchurch, L.G. Monahan & E.J.

855 Harry, (2012) 3D-SIM Super Resolution Microscopy Reveals a Bead-

856 Like Arrangement for FtsZ and the Division Machinery: Implications for

857 Triggering Cytokinesis. *PLoS biology* **10**.

858 Szwedziak, P., Q. Wang, T.A. Bharat, M. Tsim & J. Lowe, (2014) Architecture

859 of the ring formed by the tubulin homologue FtsZ in bacterial cell

860 division. *Elife* **3**: e04601.

861 Trip, E.N. & D.J. Scheffers, (2015) A 1 MDa protein complex containing

862 critical components of the *Escherichia coli* divisome. *Scientific reports*

863 **5**: 18190.

864 Vicidomini, G., G. Moneron, K.Y. Han, V. Westphal, H. Ta, M. Reuss, J.

865 Engelhardt, C. Eggeling & S.W. Hell, (2011) Sharper low-power STED

866 nanoscopy by time gating. *Nature methods* **8**: 571-573.

867 Vicidomini, G., A. Schonle, H. Ta, K.Y. Han, G. Moneron, C. Eggeling & S.W.

868 Hell, (2013) STED nanoscopy with time-gated detection: theoretical

869 and experimental aspects. *PLoS One* **8**: e54421.

870 Weiss, D.S., (2015) Last but not least: new insights into how FtsN triggers

871 constriction during *Escherichia coli* cell division. *Molecular microbiology*

872 **95**: 903-909.

873 Wissel, M.C. & D.S. Weiss, (2004) Genetic analysis of the cell division protein

874 FtsI (PBP3): amino acid substitutions that impair septal localization of

875 FtsI and recruitment of FtsN. *Journal of bacteriology* **186**: 490-502.

876   Xiao, J. & E.D. Goley, (2016) Redefining the roles of the FtsZ-ring in bacterial

877   cytokinesis. *Current Opinion in Microbiology* **34**: 90-96.

878   Yang, X., Z. Lyu, A. Miguel, R. McQuillen, K.C. Huang & J. Xiao, (2017)

879   GTPase activity-coupled treadmilling of the bacterial tubulin FtsZ

880   organizes septal cell wall synthesis. *Science* **355**: 744-747.

881   Yao, Q., A.I. Jewett, Y.W. Chang, C.M. Oikonomou, M. Beeby, C.V. Iancu, A.

882   Briegel, D. Ghosal & G.J. Jensen, (2017) Short FtsZ filaments can

883   drive asymmetric cell envelope constriction at the onset of bacterial

884   cytokinesis. *EMBO J.*

885

886

887

888   **Figures legends**

889

890   **Figure 1. Radial separation of FtsZ and FtsN during constriction of the**

891   **cell envelope in *E. coli*.** (**A**) Cells engineered to express fluorescently

892   labeled division proteins were trapped in micron-sized holes in agarose beds

893   so that divisome proteins could be imaged through the longitudinal axis of the

894   cell. For more information see Supporting Information Fig. S1. Cells co-

895   expressing (**B**) FtsZ-GFP/mCherry-FtsN   (n = 51), (**C**) FtsZ-mNG/mCherry-

896   FtsN   (n = 72), (**D**) ZipA-GFP/mCherry-FtsN (n = 54) and (**E**) GFP-

897   FtsI/mCherry-FtsN (n = 30) were trapped in microholes and imaged by SIM.

898   Left column shows cells where the radius of the division ring was > 450 nm.

899   Right column, cells where the radius of the division ring was < 450 nm. Next

900   to each image are the corresponding fluorescence intensity line scans. These

901   scans start at 9 o'clock in each image (see red triangle in (**B**)) Scale bars =

902   0.5 µm. (**F**) Comparison between the radius of mCherry-FtsN and either FtsZ-

903   GFP or ZipA-GFP (n > 45). Trend line for FtsZ-GFP /mCherry-FtsN; y = 0.89x

904   + 72.2 ($r_{Pearson}$ = 0.973, p < 0.05). Trend line for ZipA-GFP /mCherry-FtsN; y =

905   0.86x + 91.7 ($r_{Pearson}$ = 0.982, p < 0.05). n > 50 for both pairs. (**G**) Comparison

906   between GFP-FtsI and mCherry-FtsN radii throughout constriction. Trend line

907   mCherry-FtsN/GFP-FtsI; y = 1.01x+0.42 ($r_{Pearson}$ = 0.999, p < 0.05). n = 30.

908   (**H**) Summary of the separation between various divisome proteins during

909   different stages of constriction. y-axis shows average difference in radius

910   between mCherry-FtsN and respective protein (in nm). Bar graphs show

911   averaged data; At least 50 cells from FtsZ-GFP /mCherry-FtsN and 30 cells

912   from ZipA-GFP /mCherry-FtsN. Error bars indicate SEM. All strains had

913   comparable lengths and widths to a wild type strain and their generation times

914   appeared unaffected. Controls for cell length, width and growth can be found

915   in Supporting Information Fig. S2.

916

917   **Figure 2. Separation between FtsZ and FtsN resolved at nanometer scale**

918   **by dual-color gSTED.** (**A**) Cells co-expressing FtsZ-mNG and mStrawberry-

919   FtsN were trapped in microholes, fixed and imaged by dual-color gSTED.

920   Red arrow indicates the start of the fluorescence line trace. The graph on the

921   right-hand panel shows the intensity of each fluorescent protein around the

922   circumference of the division site. For comparison, a representative line in a

923   live/unfixed cell is shown in Supporting Information Fig. S8. (**B**) Close up

924   images of a ring section highlighting areas where the fluorescence signals

925   from FtsZ-mNG and mStrawberry-FtsN were the same radii but not

926   overlapping. Dotted white line indicates fluorescence line trace, starting at the

927   red arrow. (**C**) Close up images of a ring section where FtsZ-mNG and

928   mStrawberry-FtsN have constricted to different radii. Differences are

929   highlighted through fluorescence line traces in the graphs. Line (1) shows

930   FtsZ densities aligned along the circumference of the membrane. Line (2)

931   shows a density that is perpendicular to the membrane. Positive x direction

932   indicates increasing radii. (**D - G**) Pseudo time-lapse images of cells co-

933   expressing FtsZ-mNG and mStrawberry-FtsN. The cells were trapped in

934   microholes and imaged by dual-color gSTED. Radii denoted are those

935   measured for FtsZ-mNG. Scale bars (**A**) and (**D - G**) = 0.5 µm, (**B**) and (**C**) =

936   0.1 µm

937

938   **Figure 3. Septal organization of divisome proteins revealed by gSTED.**

939   (**A**) Cells expressing FtsZ-mNG were trapped in microholes, fixed and imaged

940   at different stages of constriction by gSTED. For comparison, live/unfixed cells

941   are shown in Supporting Information Fig. S10. (**B**) Distribution of fluorescent

942   density lengths obtained from gSTED images of FtsZ-mNG (n = 55). (**C**) An

943   example of an FtsZ-mNG density that was not positioned along the

944   circumference of the cell. (**D**) Wild type cells were fixed and then trapped in

945   microholes. FtsZ was subsequently labelled using anti-sera and imaged at

946   different stages of constriction by gSTED. (**E**) Distribution of fluorescent

947   density lengths obtained from gSTED images of antibody labeled FtsZ (n =

948   51). (**F**) An example of a density that was not positioned along the

949   circumference of the cell. (**G**) Cells expressing mCitrine-FtsN were trapped in

950   microholes, fixed and imaged at different stages of constriction by gSTED. (**H**)

951   Distribution of fluorescent density lengths obtained from gSTED images of

952   mCitrine-FtsN (n = 59). (**J**) An example of mCitrine-FtsN density that was not

953   positioned along the circumference of the cell. (**K**) Wild type cells were fixed

954   and then trapped in microholes. FtsN was labelled using anti-sera and imaged

955   at different stages of constriction by gSTED. (**L**) Distribution of fluorescent

956   density lengths obtained from gSTED images of antibody labeled FtsN (n =

957   53). (**M**) Close up of typical arrangement of native FtsN densities along the

958   circumference of the ring. (**N**) Summary of measured density lengths. (**O**)

959   Average ring coverage in % of FtsZ and FtsN at septum in unconstricted cells

960   (100 % would indicate full ring coverage). FP = Fluorescent Protein. IFM =

961   Immunofluorescence. For consistency all images were pseudo-colored green

962   irrespectively of their emission wavelength. Bin width for the histograms in

963   (**B**), (**E**), (**H**) and (**L**) is 25 nm. Full Width at Half Maximum (FWHM) in the

964   graphs indicates the thickness of the filament. Scale bars = 0.5 µm.

965

966   **Figure 4. FtsN moves around the division septum even after it has**

967   **separated from FtsZ.** Cells simultaneously expressing FtsZ-GFP and

968   mCherry-FtsN were analyzed using time-lapse SIM. (**A**) Representative

969   images of a cell with overlapping fluorescence signals. (**B**) Representative

970   images a cell where signals did not overlap. Numbers in top right corners

971   indicate the time after the first shown image. Next to each image are 3D

972   surface plots that highlight the variation in fluorescence intensity along the

973   circumference of the rings between each time point. See also Supporting

974   Movies S1 and S2.

975

976   **Figure 5. Different modes of subunit exchange between FtsZ and FtsN at**

977   **septum.** (**A**) Confocal FRAP measurements of cells simultaneously

978   expressing FtsZ-mNG and mCherry-FtsN. The boxed region was photo-

979   bleached and the recovery of fluorescence monitored at times indicated.

980   Recovery curves for FtsZ-mNG (green) and mCherry-FtsN (red) are shown in

981   (**B**). (**C**) Quantification of recovery times for bleached half-rings of various

982   divisome proteins. Examples of raw data are shown in Supporting Information

983   Fig. S15. (**D**) Following bleaching the reappearance of FtsZ-GFP in filaments

984   was tracked over time. These filaments reappeared throughout the bleached

985   areas (see also Supporting Movie S5). (**E**) As for panel D except that FtsZ-

986   mNG was used. (**F**) After bleaching the reappearance of mCitrine-FtsN was

987   monitored over time. The fluorescence reappeared throughout the bleached

988   areas (i.e. no transient filament like structures were observed). Scale bars =

989   0.5 µm.

990

991   **Figure 6. Increasing radial distance between FtsZ and FtsN during**

992   **constriction.** Model depicting how the spatial difference between FtsZ and

993   FtsN changes with constriction of the septum. (**A**) Prior to the initiation of

994   constriction the radii of the two 'rings' essentially overlap. However, the FtsZ

995   filaments and FtsN assemblies do not always co-localize circumferentially. (**B**)

996   As constriction of the cell envelope advances, the radial difference between

997   FtsZ and FtsN increases to, on average, 50 nm. OM, outer membrane; IM,

998   inner membrane; PG, peptidoglycan.

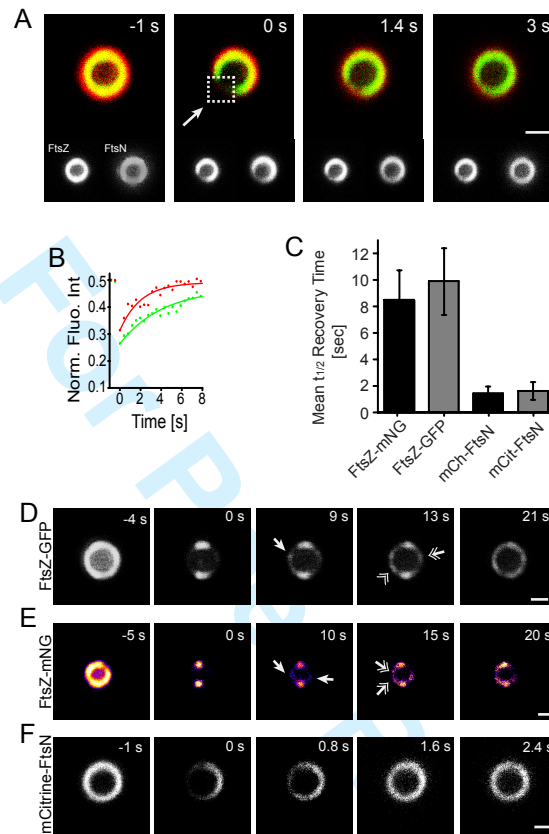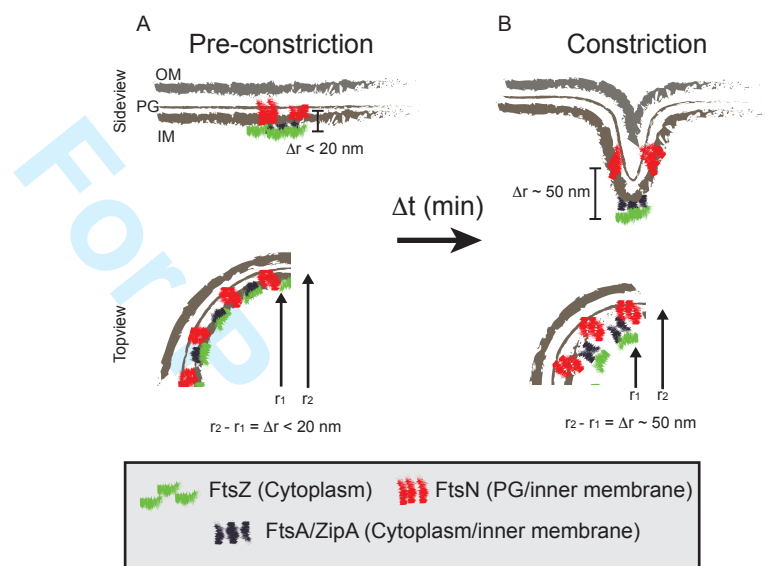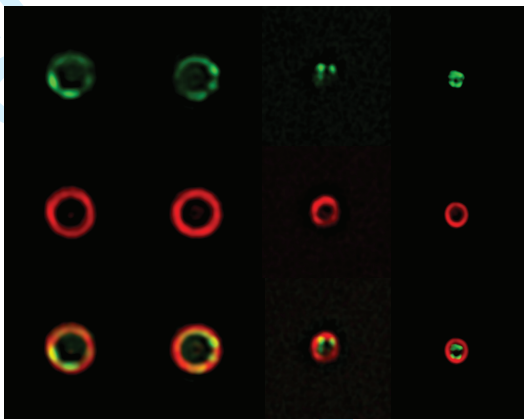Figure 1
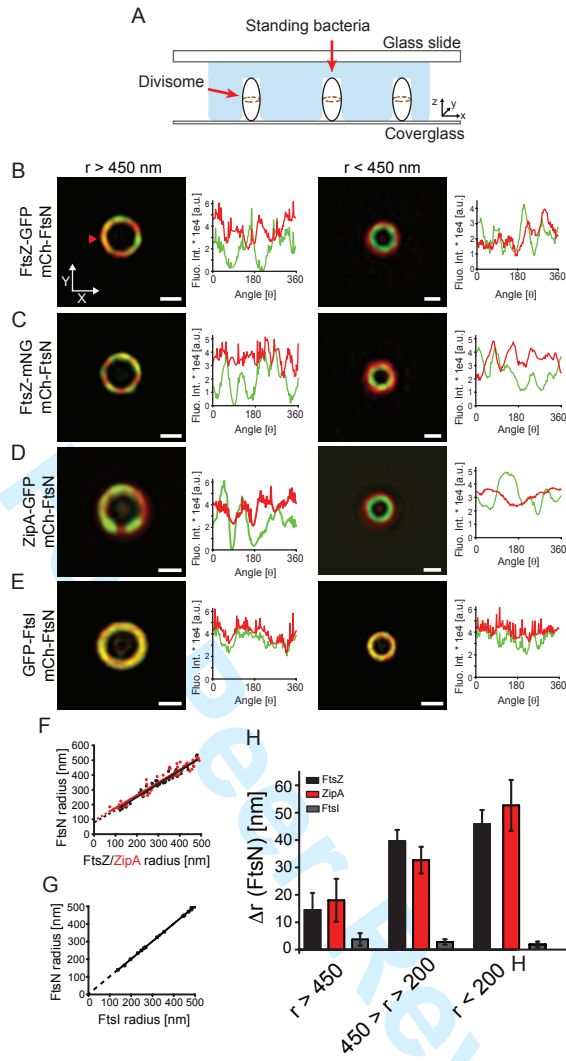
Figure 2
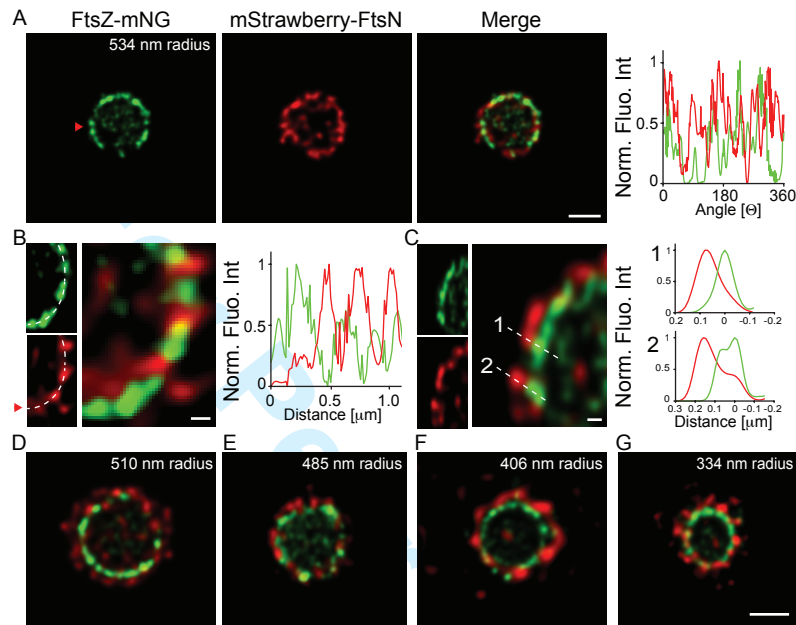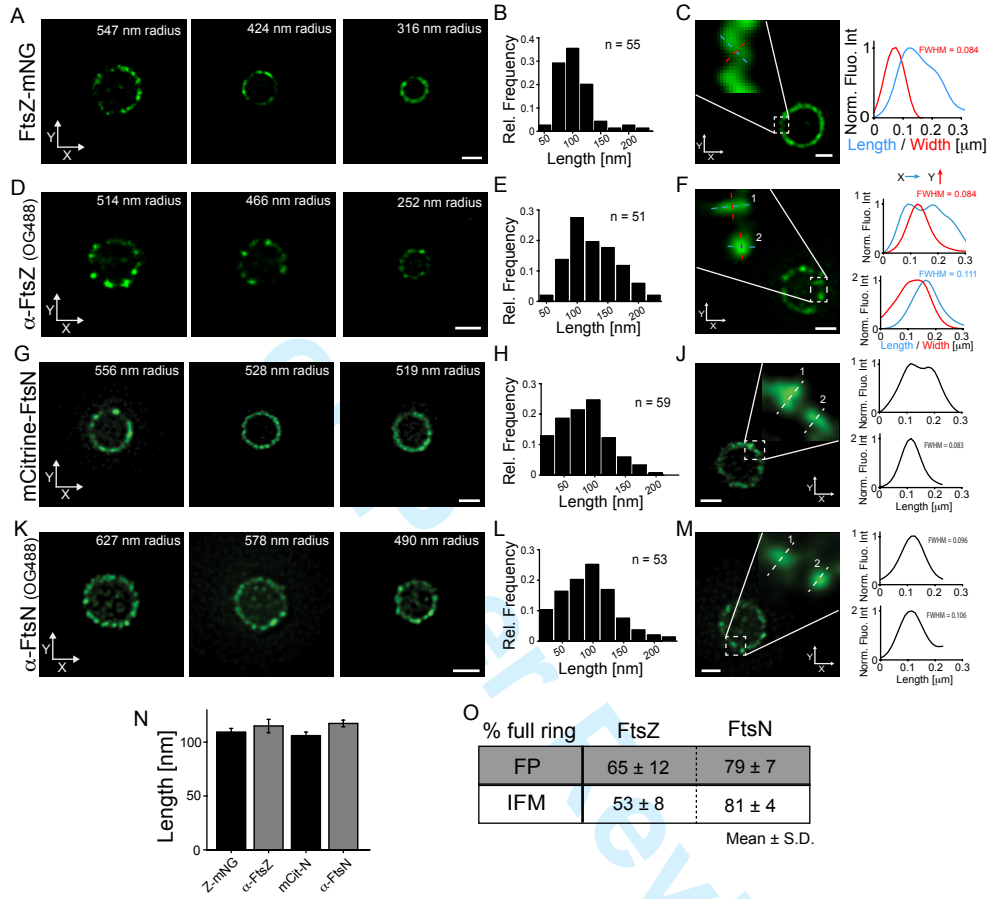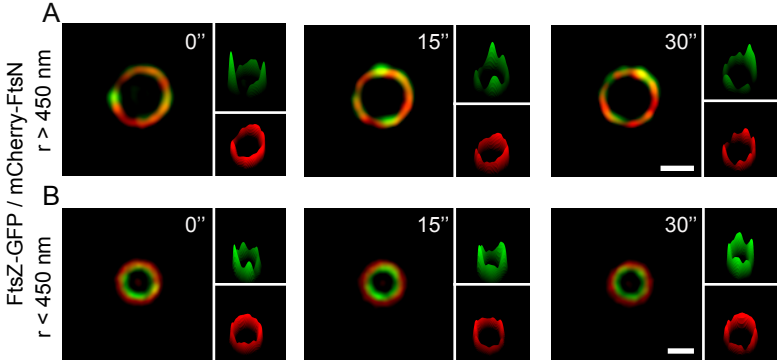
Figure 3

Figure 4

Figure 5

Figure 6

Abbreviated summary

In order to divide, bacterial cells assemble a macromolecular machine, termed 'the divisome'. Herein we used super-resolution microscopy investigate the organization of two key divisome proteins; FtsZ and FtsN. We found that these proteins were both circumferentially and radially separated into individual protein assemblies. Thus, our data indicates that division is brought about by a collection of independently operating protein assemblies, rather than a single macromolecular machine.

2
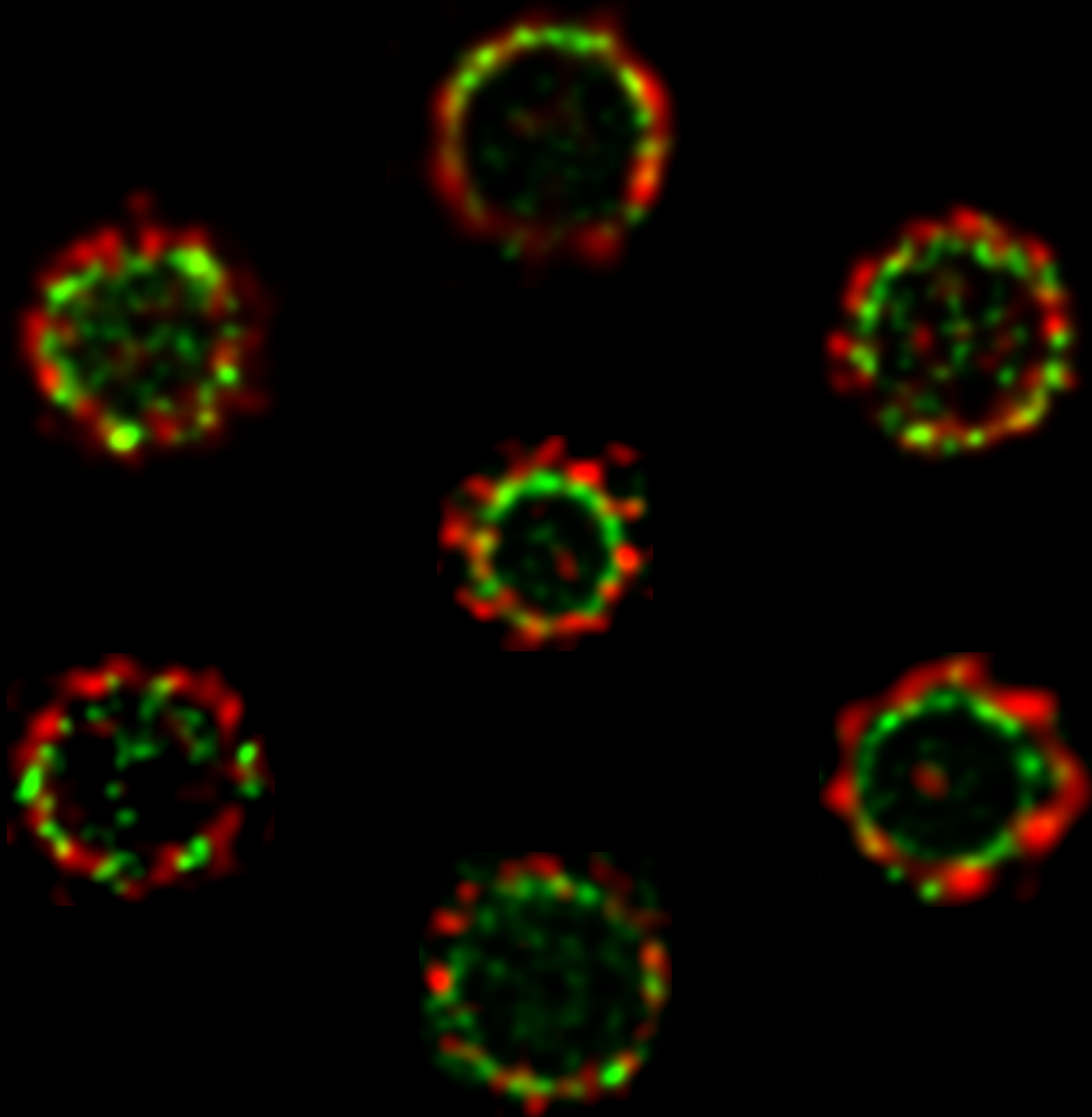
A montage of images through the division septum of *E. coli* cells. The images were captured by dual-color time-gated Stimulated Emission Depletion (STED) nanoscopy, on cells simultaneously expressing FtsZ-mNeonGreen (green) and mStrawberry-FtsN (red). The images show that FtsZ and FtsN are spatially separated.